A Computer Model of Human Atria With Reasonable Computation Load and Realistic Anatomical Properties

Olivier Blanc, Nathalie Virag*, Jean-Marc Vesin, *Member, IEEE*, and Lukas Kappenberger

***Abstract*—Atrial fibrillation is the most frequent arrhythmia, provoking discomfort, heart failure and arterial embolisms. The aim of this work is to develop a simplified anatomical computer model of human atria for the study of atrial arrhythmias and the understanding of electrical propagation mechanisms. With the model we propose, up to 40 s of real-time propagation have been simulated on a single-processor computer. The size and the electrophysiological properties of the simulated atria are within realistic values and information about anatomy has been taken into account in a three-dimensional structure. Besides normal sinus beat, pathological phenomena such as flutter and fibrillation have been induced using a programmed stimulation protocol. One important observation in our model is that atrial arrhythmias are a combination of functional and anatomical reentries and that the geometry plays an important role. This virtual atrium can reproduce electrophysiological observations made in humans but with the advantage of showing in great detail how arrhythmias are initiated and sustained. Such details are difficult or impossible to study in humans. This model will serve us as a tool to evaluate the impact of new therapeutic strategies and to improve them.**

***Index Terms*—Atrial arrhythmias, computer modeling, electrical propagation, fibrillation, flutter, human atria.**

I. Introduction

THE most frequent cardiac arrhythmias in humans are related to the atria. Furthermore, atrial fibrillation (AF) often provokes disabling symptoms and severe complications such as heart failure and stroke [1]. However, even if one can obtain experimental details on many of the relevant complex electrophysiological processes initiating or sustaining atrial arrhythmias, there is no reliable model to test therapeutic interventions. Today, some of the treatments for AF are still based on trial and error, empirical considerations, and human experiments, yet many of the underlying mechanisms remain unclear. On the other hand, as it has been shown in other fields of science, computer simulation allows one to simulate experiments that cannot be performed *in vivo* [2]. This approach gives further insight on the phenomena involved in cardiac arrhythmias and gives the possibility to test and improve therapeutic interventions. However, its success relies on the fact that the computer model of the heart represents a reasonable approximation of the real electrophysiological behavior.

The development of a realistic three-dimensional (3-D) model of the whole heart, incorporating an accurate representation of anatomy and cellular biophysics, is difficult today due to the high computation time required [2]. Since the available computer power is limited, the most effective computer models of electrical propagation in the heart based on detailed ionic models have up to 1 000 000 elements [3], [4], which limits the size of tissue that can be simulated. Each computer model requires a compromise between the following parameters: complexity of the cellular membrane model, complexity of the cardiac tissue structure (monodomain or bidomain), size of tissue, and number of spatial nodes, complexity of the represented anatomy, duration of the simulated events, stability and accuracy of the numerical method. Therefore, typical models consist of sophisticated two-dimensional (2-D) patches of only a few square centimeters of cardiac tissue, or 3-D models taking into account anatomy but with an extremely simplified cellular behavior, or 3-D model taking into account sophisticated anatomical and electrophysiological features but limited to the simulation of normal propagation.

Since the most fatal arrhythmias leading to sudden death are of ventricular origin, most research efforts in electrophysiology and computer modeling are directed toward understanding ventricular tachycardias and ventricular fibrillation. Very few models have been developed to study AF despite the fact that such arrhythmias are more frequent. Atrial geometry is known to be a key factor for the development of atrial arrhythmias, therefore atrial models have to include this aspect [5], [6]. To overcome this problem, most computer models incorporating anatomic properties use simplified cellular models, such as the FitzHugh–Nagumo model [5], [7]. However if we consider that, in contrast to the ventricular myocardium, atria have a limited surface and wall thickness, this assumption should allow the development of a realistic model taking into account both anatomical and electrophysiological properties with today's computer power.

In this paper, we present a computer model of human atria having a 3-D structure and modeling those two aspects above. In order to obtain simulation results that are comparable to clinical experiments, we have chosen to develop a model capable of simulating atrial arrhythmias during several seconds in a tissue with realistic size. To achieve this goal, we selected simplified

Manuscript received September 28, 2000; revised July 2, 2000. This work was supported by grants from the Theo-Rossi-Di-Montelera Foundation, Medtronic Europe S.A. and the Swiss Governmental Commission of Innovative Technologies (CTI). *Asterisk indicates corresponding author*

O. Blanc and J.-M. Vesin are with the Signal Processing Laboratory, Swiss Federal Institute of Technology, 1015 Lausanne, Switzerland.

*N. Virag is with Medtronic Europe SA, Route du Molliau, CH-1131 Tolochenaz, Switzerland (e-mail: nathalie.virag@medtronic.com).

L. Kappenberger is with the Division of Cardiology, CHUV, 1011 Lausanne, Switzerland.

Publisher Item Identifier S 0018-9294(01)09138-8.

cellular ionic models (the Beeler–Reuter [8] and the Luo–Rudy models [9]), a simplified tissue structure (a monodomain model [2]) and implemented a 3-D structure with only one layer of cells. Furthermore, we took into account only the effect of the large anatomical obstacles created by the veins and the valves. This was motivated by the fact that atrial orifices are known to play an important role in the initiation and perpetuation of atrial arrhythmias [10]–[12]. The objective of this paper is to demonstrate that, although this model is a simplification of reality, it can contribute to the understanding of atrial arrhythmias and provide a tool for the development of therapeutic strategies.

II. Methods

A. Model of Cardiac Tissue

A 2-D model of cardiac tissue is composed of two major components: a model for the ionic kinetics of the atrial cells (model of excitation) and a model of interconnection between the cells (resistors). The choice of a particular model of excitation is determined by the degree of accuracy desired for the simulations and the available computer power. Most large-scale models of complex geometries use simplified cellular models such as cellular automata [13] or two state variable models like the FitzHugh–Nagumo models [14]. Those models are well suited for simulations on a high number of cells but provide only a simplified and dimensionless approximation of the action potential. More sophisticated models are based on a quantitative description of ionic currents through the cell membrane from eletrophysiological experiments. Such membrane models have been developed for different cells like the sinoatrial cells [4], [15], atrial cells [4], [16] and ventricular cells [8], [9], [17]. Since they are based on physiological parameters, they are well suited for the study of arrhythmias. We have chosen to work with the well-known ionic models developed by Beeler–Reuter [8] and Luo–Rudy [9]. They have been validated for ventricular cells, but as a first approximation, we will be using them for an atrial tissue. Indeed, the general behavior is similar. Furthermore, the very sophisticated membrane models available for atrial cells do not allow the construction of the whole atria or the simulation of time frames of several seconds with today's computer power. This remark is also valid for the second version of the Luo–Rudy model [17], which contains ion pumps and exchangers.

Electrical propagation through the cardiac tissue is known to involve both the intracellular and the extracellular compartments (bidomain model [18]). However, since the extracellular domain has a much higher conductivity than the intracellular domain, we can reduce the computation time by assuming that the extracellular domain is grounded, implementing therefore a monodomain model. The electrical propagation through the cardiac tissue is described in the general case by the following reaction-diffusion equation in the intracellular domain:

$$\frac{1}{S_v}\nabla\cdot(D\nabla V_m) = C_m\frac{\partial V_m}{\partial t} + I_{\text{ion}} - I_{\text{stim}} \qquad (1)$$

where

- V_m transmembrane potential;
- S_v surface to volume ratio;
- D conductivity tensor;
- C_m membrane capacitance;
- I_{ion} sum of the transmembrane ionic currents described in our case either by the Beeler–Reuter or the Luo–Rudy models;
- I_{stim} transmembrane stimulus current that can be applied externally to initiate propagation in the tissue.

The parameters S_v and C_m are related to passive tissue properties and are assumed to be constant over time and space (all the simulations presented in this paper were conducted with $C_m = 1\ \mu$ F/cm^2 and $S_v = 0.24\ \mu$m^{-1}). The values of intracellular resistivities in the longitudinal and transverse directions can be individually programmable for each cell via the conductivity tensor D, allowing us to introduce heterogeneities in the cardiac tissue (ischemic zones, anatomical structures, obstacles to conduction). Anisotropy can be also introduced along the two principal directions. The electrical propagation in this 2-D cardiac tissue has been described in a previous work [19].

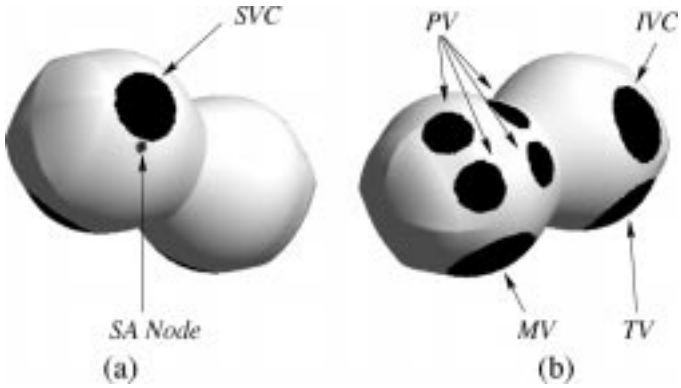

Fig. 1. Geometrical model proposed for human atria, with orifices represented in black: (a) anterior view with superior vena cava (SVC) and sinoatrial node (SA node) visible in right atrium, (b) posterior view with inferior vena cava (IVC) and tricuspid valve (TV) in right atrium, four pulmonary veins (PV) and mitral valve (MV) visible in left atrium.

B. Model of Atrial Geometry

Based on the assumption that atria have a limited wall thickness, we propose in this paper a realistic atrial model obtained by folding the 2-D cardiac tissue described in Section II-A into a 3-D structure. The 3-D shape that is used here as an approximation of the atrial geometry consists of two ellipsoids of a diameter of 35 mm connected together and with an overall length of 80 mm. The data are computed on a 2-D sheet assembly representing an unfolded box made of three rectangular patches connected together with periodic boundary conditions. They are then mapped onto the final geometry, while keeping the distortion in a range that does not alter the propagation properties.

Our purpose is to obtain a good topological equivalence between the real human atria and the proposed atrial geometry using a simplified model. Therefore, orifices of appropriate size and location have been placed to simulate the veins and the valves (Fig. 1).

The structure has a surface of 100 cm^2 with the orifices for the veins and valves representing 20% of this area. The surface of the mitral valve (MV) and the tricuspid valve (TV) is 4 cm^2, 2 cm^2 for the superior vena cava (SVC), 2.5 cm^2 for the inferior

vena cava (IVC) and 1 cm^2 for each of the four pulmonary veins. These value are comparable to those found in human atria [20], [21]. The sinoatrial (SA) node is defined anatomically at the SVC right atrial junction. No conduction is assumed through the septum (since its electrophysiological properties and anatomical extent remain controversial) and other local tissue characteristics have not been taken into account. In particular, we simplified the tissue and considered an isotropic and homogeneous tissue (except for the anatomical obstacles). In this case, the conductivity tensor D can be expressed as a function of the global tissue resistivity ρ

$$D = \frac{1}{\rho}\begin{bmatrix} 1 & 0 \\ 0 & 1 \end{bmatrix}. \tag{2}$$

Even if this model is simplified, it represents a realistic approximation of the atrial topology, size, and electrophysiology. It combines the advantages of the low computational load provided by 2-D tissue models [3], [22] with some advantages of anatomical 3-D models [23].

C. Numerical Method

A semi-implicit centered scheme (Crank-Nicholson [24]) has been used to integrate (1) in two dimensions. The term $(\partial V_m/\partial t)$ is approximated by $\left(V_m^{i,j,t+\Delta t} - V_m^{i,j,t}\right)/\Delta t$, with Δt the time discretization, and the average of the values at times t and $t+\Delta t$ are taken for the central difference in space

$$\begin{aligned}
&\frac{1}{2S_v\Delta x^2}\left(\frac{V_m^{i+1,j,t}-V_m^{i,j,t}}{\rho^{(i+1)\to i,j}}+\frac{V_m^{i-1,j,t}-V_m^{i,j,t}}{\rho^{(i-1)\to i,j}}\right)\\
&+\frac{1}{2S_v\Delta x^2}\\
&\times\left(\frac{V_m^{i+1,j,t+\Delta t}-V_m^{i,j,t+\Delta t}}{\rho^{(i+1)\to i,j}}+\frac{V_m^{i-1,j,t+\Delta t}-V_m^{i,j,t+\Delta t}}{\rho^{(i-1)\to i,j}}\right)\\
&+\frac{1}{2S_v\Delta y^2}\\
&\times\left(\frac{V_m^{i,j+1,t}-V_m^{i,j,t}}{\rho^{i,(j+1)\to j}}+\frac{V_m^{i,j-1,t}-V_m^{i,j,t}}{\rho^{i,(j-1)\to j}}\right)\\
&+\frac{1}{2S_v\Delta y^2}\\
&\times\left(\frac{V_m^{i,j+1,t+\Delta t}-V_m^{i,j,t+\Delta t}}{\rho^{i,(j+1)\to j}}+\frac{V_m^{i,j-1,t+\Delta t}-V_m^{i,j,t+\Delta t}}{\rho^{i,(j-1)\to j}}\right)\\
&\quad = C_m\frac{V_m^{i,j,t+\Delta t}-V_m^{i,j,t}}{\Delta t}+I_{\text{ion}}^{i,j,t}-I_{\text{stim}}^{i,j,t+\Delta t}
\end{aligned} \tag{3}$$

where

i and j	spatial indexes of discrete nodes in the x and y directions;
$\rho^{(i+1)\to i,j}$	resistivity between nodes $(i+1,j)$ and (i,j);
Δx and Δy	spatial discretization.

The propagation process is solved iteratively in time, by separating its reaction and diffusion parts. First, the ionic currents $I_{\text{ion}}^{i,j,t}$ are computed for each cardiac cell at time t using the Beeler–Reuter or Luo–Rudy formulation. Lookup tables were used to compute the gating parameters. Second, the transmembrane potentials $V_m^{i,j,t+\Delta t}$ are updated using (3). This second step is computationally expensive and is solved with the alternate-direction implicit (ADI) technique, which has the advantage of using tridiagonal matrices for the resolution of the system of equations [24]. The choice of an implicit scheme over an explicit one was motivated by the unconditional stability of the diffusion part and improved accuracy [25], at the expense of having to solve a set of simultaneous equations at each time step.

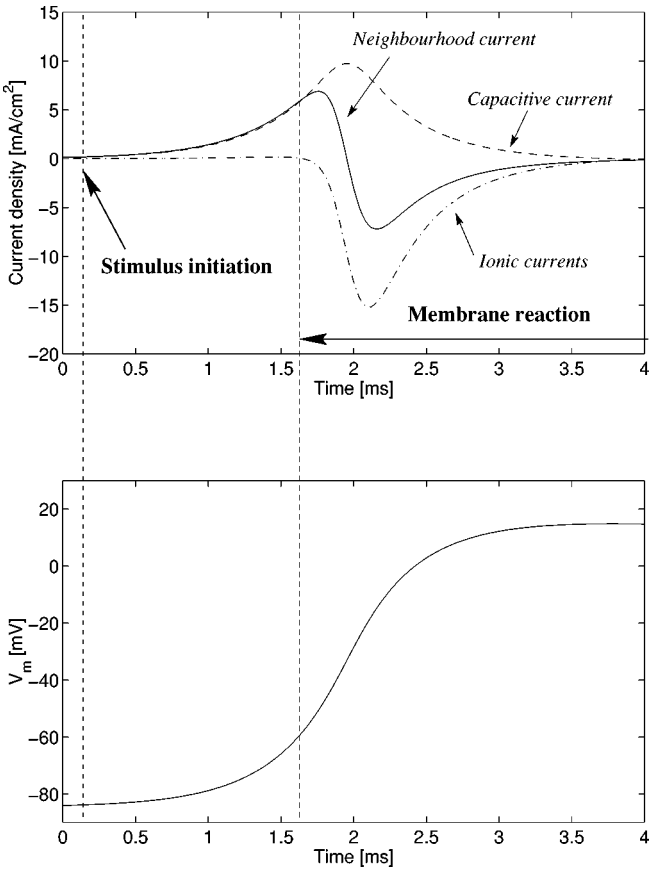

Fig. 2. Representation of the temporal evolution of the three main current contributions and the corresponding transmembrane potential for a single cell connected to its four neighbors (zoom on the upstroke of the depolarization process, Beeler–Reuter model).

D. Spatial and Temporal Discretization

The choice of the time (Δt) and spatial discretizations (Δx and Δy) in (3) is the result of a tradeoff between computation speed and accuracy (as well as stability in the case where an explicit scheme is being used for integration). Due to the nonlinear and stiff characteristics of propagation equations, numerical errors introduced by discretizing the continuous (1) exhibit a nonlinear dependence with respect to the temporal and spatial steps used to integrate it. This problem of spatial discretization and its consequences in the case of one-dimensional propagation have been deeply investigated by Wu and Zipes in [26]. In our case, we have a 2-D model, and spatial discretization affects not only the propagation properties but also the reentry dynamics.

The main limitation to a decrease of computational load by an increase of the spatial and temporal discretizations is determined by the upstroke of the depolarization of the transmembrane potential V_m. This critical phase is represented in Fig. 2

using the Beeler–Reuter model. The three currents involved in (1) are represented during the upstroke, together with the corresponding temporal evolution of V_m. First, the propagation is initiated by injecting an intracellular stimulus current I_{stim} and is maintained by the intracellular neighborhood currents coming from the adjacent cells and represented by the Laplacian term $(1/S_v)\nabla \cdot (D\nabla V_m)$. These currents are then integrated by the cell membrane capacitance (capacitive current $C_m(\partial V_m/\partial t)$) leading to a progressive increase of the cell transmembrane potential V_m until a threshold is reached, that provokes a fast response of the inward sodium current and the apparition of ionic currents (membrane reaction). One can observe that the neighborhood currents represented by the Laplacian term are significant in (1) only during the upstroke phase of the action potential represented in Fig. 2. Therefore, after this upstroke, the temporal evolution of a given cell is almost independent of its neighbors and spatial discretization becomes less critical. Temporal discretization is mostly determined by an appropriate discretization of the fast inward sodium current, which is the ionic current with the fastest dynamics.

A bad approximation of the Laplacian term $(1/S_v)\nabla \cdot (D\nabla V_m)$ by a coarse spatial discretization will result in an altered propagation velocity that can lead to propagation artifacts. This is shown in Fig. 3 both for the spatial and temporal (also represented in Fig. 2) evolutions. Fig. 3 shows the effect of spatial discretization on: 1) the excitation currents coming from neighboring cells (spatial domain) and 2) the integration over time for one point in the space domain of such currents (depolarization process). Both representations can be linked using propagation velocity: if we assume a propagation velocity of 100 cm/s for example, a 1-ms upstroke will be spread over 1 mm. Therefore, if the propagation velocity is decreased, one can expect sharper spatial gradients during the upstroke and spatial discretization should be refined. The effect of a coarse approximation of the Laplacian term will always induce distortion and reduce the maximal amplitude reached by the discrete Laplacian, provoking an artificial time delay of the membrane ionic reaction and introducing several numerical errors. One can expect longer delays for coarser discretization, leading to a progressively reduced conduction velocity and finally to an artificial numerical block of propagation. Another related effect is called orthotropic anisotropy: the blocking effect has a larger influence in the direction of the discretization grid than in other directions. This error has two practical consequences: the appearance of square waves (maybe the most recognizable signature of an inappropriate discretization) and the modification of the reentry dynamics affecting the propagation of spiral wave tips, whose movements are affected by the grid directions.

In conclusion, the constraints described above on the temporal and spatial discretizations, together with the limited available computer power, impose restrictions on the numerical implementation of a computer model of atria. The propagation velocities in the human atria range from 50 cm/s to 130 cm/s in a healthy tissue [12], and can be lower in diseased areas. Fig. 4 summarizes the numerical errors on the propagation velocity resulting from different spatial discretizations (the solid line represents the case of a very fine spatial discretization). Based on the hypothesis that propagation velocity will not be slower in the atrial tissue than 30 cm/s, we chose a spatial discretization

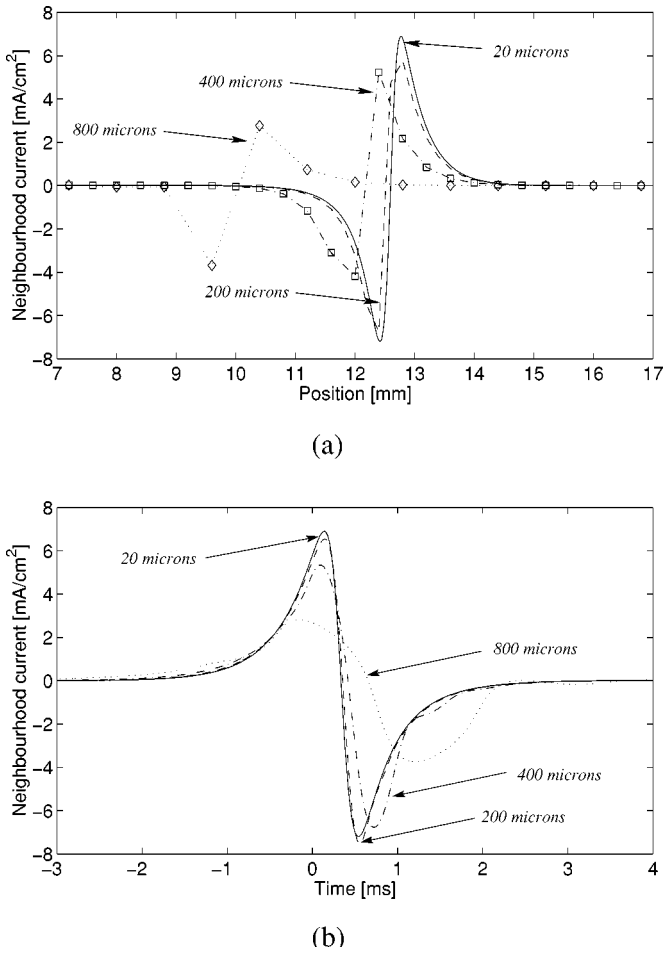

Fig. 3. Effect of different spatial discretizations on the Laplacian term $(1/S_v)\nabla \cdot (D\nabla V_m)$ (neighborhood currents) computed on a planar propagating wavefront traveling at velocity $c = 88$ cm/s ($\rho = 120\ \Omega\cdot$ cm) for one node with four neighbors and the Beeler–Reuter model. (a) Spatial evolution at a given time $t = 15$ ms. (b) Temporal evolution at a given point in space with the time origin corresponding to V_m crossing the -60-mV excitability threshold.

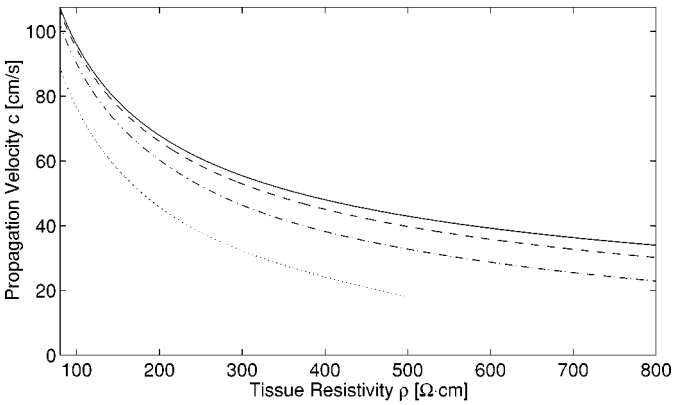

Fig. 4. Relationship between the propagation velocity and the resistivity for different spatial discretizations using the Beeler–Reuter model: (solid line) 20 μm, (dashed line) 200 μm, (dotted–dashed line) 400 μm, and (dotted line) 800 μm. On can observe the extreme case of apparition of a block of propagation due to a coarse spatial discretization for $\Delta x = \Delta y = 800\ \mu$m for propagation velocities lower than 20 cm/s.

of $\Delta x = \Delta y = 200$ μm, leading to an error on the propagation speed of less than 8% in the worst situation. This discretization applied on the simplified atrial geometry described in Section II-B produces about 250 000 nodes. The temporal discretization needed for an appropriate representation of the fast sodium current in the Beeler–Reuter model is $\Delta t = 25$ μs.

E. Computer Implementation

This model has been implemented with double precision in C++ on standard PCs. Computation load is the main limitation to the implementation of a detailed computer model of human atria. The CPU load $\mathrm{CPU_L}$ can be approximated as the product of the number of temporal steps n_T times the total number of spatial nodes n_S defining the geometrical model

$$\mathrm{CPU_L} = n_\mathrm{T} \cdot n_\mathrm{S} = \frac{T}{\Delta t} \cdot \frac{S_d}{\Delta x^d} \tag{4}$$

where T is the real-time duration of simulated frames, S_d is the size of the spatial domain of dimension d (1, 2, or 3). Therefore, for a 2-D model, a refinement of Δt by a factor of two increases $\mathrm{CPU_L}$ by the same factor, while the same refinement on $\Delta x = \Delta y$ increases $\mathrm{CPU_L}$ by a factor four. Based on these considerations, one can note that modeling the human atria with a realistic size using the Beeler–Reuter model and a 3-D model of several layers of cells is still computationally expensive today. Furthermore, we performed simulations showing that the use of a bidomain model instead of a monodomain model generally implies a slowing of the computation speed by at least an order of magnitude.

For a model with 250 000 nodes ($\Delta x = \Delta y = 200$ μm), the computation time on one processor of a Pentium III 500 MHz takes 16 h/s of simulated time, and the RAM occupied by the model is 250 MB. We are also using a second model with only 65 000 nodes ($\Delta x = \Delta y = 400$ μm) in order to obtain rapidly quantitative results (simulations take 4 h/s of simulated time and 78 MB of RAM). Finally, we can also run simulations on a model with 500 000 nodes ($\Delta x = \Delta y = 150$ μm, 32 h/s of simulated time and 400 MB of RAM).

The activation maps generated with our model are represented on the 3-D structure presented in Fig. 1. The action potential is gray-coded, dark gray representing potential values of 20 mV, and white the resting potential of -84 mV. This representation corresponds to isopotential maps. When in the form of a sequence of images, the movement of the wavefront reflects the information contained in isochrone maps.

III. Results

A. Sinus Rhythm Propagation in a Healthy Tissue

The propagation of a normal sinus beat is initiated by injecting an intracellular current I_stim into the cells situated in the SA node region. From there, the activation wavefront propagates spontaneously over the right toward the left atrial tissue. In the model of healthy tissue, the propagation speed is 90 cm/s and the action potential duration (APD) is 289 ms at a cycle length of 1000 ms (Beeler–Reuter model). This propagation is in the range of values reported for physiological tissues [12], [27]. The total activation time for both atria is 90 ms and the simulation of the normal sinus beat presented in Fig. 5 shows a realistic behavior in terms of activation maps [28]. All the simulation results presented here use the Beeler–Reuter model, but similar results could be obtained with the Luo–Rudy model.

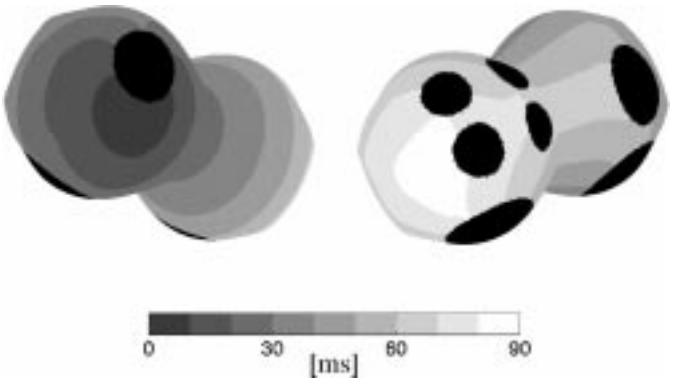

Fig. 5. Iso-activation areas during the propagation of a normal sinus beat initiated at the SA node with a propagation speed of 90 cm/s. The total activation time for both atria is 90 ms.

B. Initiation of Atrial Arrhythmias

Numerous experiments for initiating atrial arrhythmias have been performed, using a programmed stimulation protocol similar to that used for electrophysiological studies. S_1 was the basic drive impulse initiated from the SA node at a cycle length of 1000 ms. Ectopic beats S_2 and S_3 have been introduced with various coupling intervals and at several locations. In the healthy tissue, defined with a normal anatomy, size, propagation velocity and APD, most attempts to initiate an atrial arrhythmia failed, i.e., no sustained arrhythmia could be observed. Therefore, in these basic conditions, the model seems electrically stable. Arrhythmias could be initiated when the propagation speed was reduced from 90 cm/s to 30 cm/s by increasing the resistivity from $\rho = 80\,\Omega\cdot$ cm to $\rho = 800\,\Omega\cdot$ cm (Fig. 4). This decrease of propagation speed has the same effect on the simulation results as a dilation of both atria while keeping a normal propagation speed. In addition to this slow propagation, different action potential modifications have been tested by a modulation of the ionic channel. In particular, a decrease of APD by an inhibition of the Ca channel (from 10 to 50%) can in some cases facilitate reentry.

Even in a tissue with decreased propagation speed, most of the stimulation attempts have led to nonsustained arrhythmias, consisting mostly of expiring spiral waves. However, we have identified that some locations are more likely to generate a sustained reentrant wavefront. In the experiments performed so far, we have identified that the isthmus between the IVC and the TV and the region of the pulmonary veins are critical. This observation correlates with the observations obtained from human atria in [29] and in ablation techniques proposed for atrial arrhythmias.

Atrial flutter-like activity could be initiated with a normal sinus rhythm followed by one critically timed and located ectopic beat. The propagation velocity was locally decreased from 90 cm/s to 30 cm/s in the isthmus between IVC and TV and the APD was reduced from 289 ms to 113 ms uniformly through

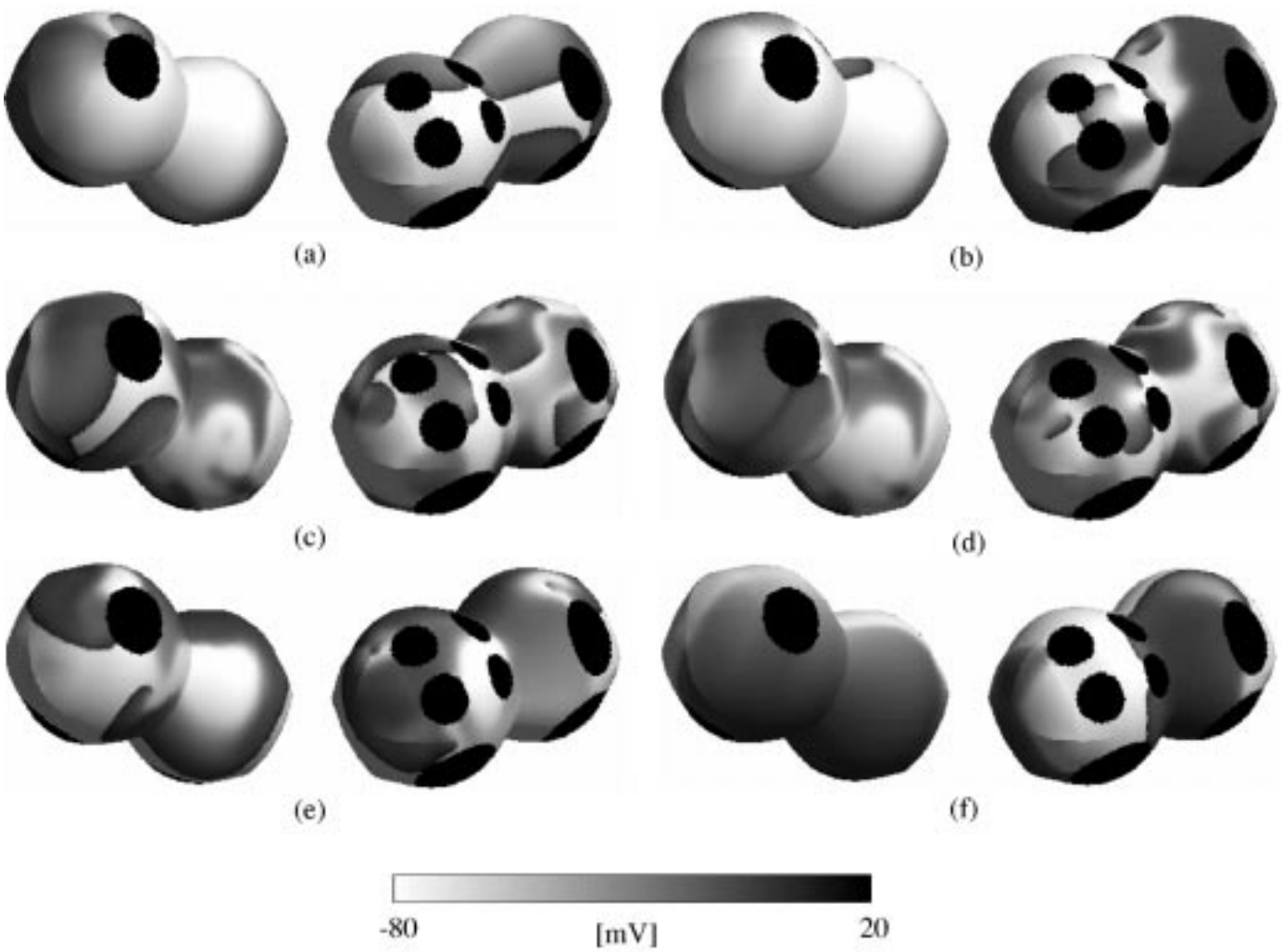

Fig. 6. Example of initiation of AF in a homogeneous tissue with a propagation speed of 30 cm/s and $\mathrm{APD} = 252$ ms. The S_1 stimulus is followed by two ectopic beats S_2 and S_3 with a coupling interval of 350 ms and 222 ms, respectively: (a) $t = 605$ ms, shortly after the application of S_3; (b) $t = 1580$ ms, just at the onset of AF; (c) $t = 4425$ ms; (d) $t = 4450$ ms, AF with up to eight independent wavelets; (e) $t = 12\,325$ ms, transition from AF to atrial flutter; and (f) $t = 14\,650$ ms, atrial flutter-like activity with a periodic pattern.

the atria. For example, with a carefully timed ectopic beat S_2 located between the IVC and the TV, we could initiate a typical atrial flutter-like reentry [12] in the form of a single counterclockwise macro-reentrant circuit with a periodic pattern and an average rate of 200 beats/minutes (bpm). The resulting wavefront is located mainly within the right atrium and the reentry circuit is closely attached to the IVC.

AF could be initiated with a normal sinus rhythm followed by two or three critically timed ectopic beats. In our model, fibrillation could only be initiated in a tissue with globally decreased propagation velocity (30 cm/s). AF could not be sustained with the normal propagation velocity of 90 cm/s because the corresponding wavelength (27 cm for an APD of 289 ms) is larger than the atrial tissue. Reduced APD facilitates fibrillation perpetuation but is not required. We have been able to initiate AFs sustained for more than 40 s (limited only by the simulation time). Interestingly, however, most AF spontaneously converted to atrial flutter or to quiescence (ready for the next sinus beat), as in biological models [10]. Fig. 6 illustrates an example of initiation of AF by two ectopic beats S_2 and S_3 located in the high right atrium with an S_1–S_2 interval of 320 ms and an S_2–S_3 of 222 ms. In this case, fibrillation lasts for about 12 s (with a temporary slower flutter-like activity in the middle of the fibrillation episode) and then finally converts to sustained atrial flutter. One can clearly see that, compared to the periodic pattern of atrial flutter, AF is observed as multiple reentering wavelets traveling randomly.

It is interesting to observe the corresponding development of the number of wavelets and the percentage of excited tissue during the initiation and the conversion of AF as shown in Fig. 7. During AF, up to eight wavelets are present and the average rate for this example is 250 bpm. This resembles the mapping data in canine and human hearts [30]. When reducing the APD, one can obtain higher average rate for AF (for example, with an APD of 160 ms, we could observe an average rate for AF of up to 420 bpm). During the spontaneous conversion to atrial flutter there is a gradual reorganization and reduction of the number of wavelets. The evolution of the percentage of excited tissue (defined as the amount of cardiac cells with a V_m greater than -60 mV) is characterized by important periodic variations in the initiation phase. During fibrillation, these variations decrease, while they increase during the transitions from fibrilla-

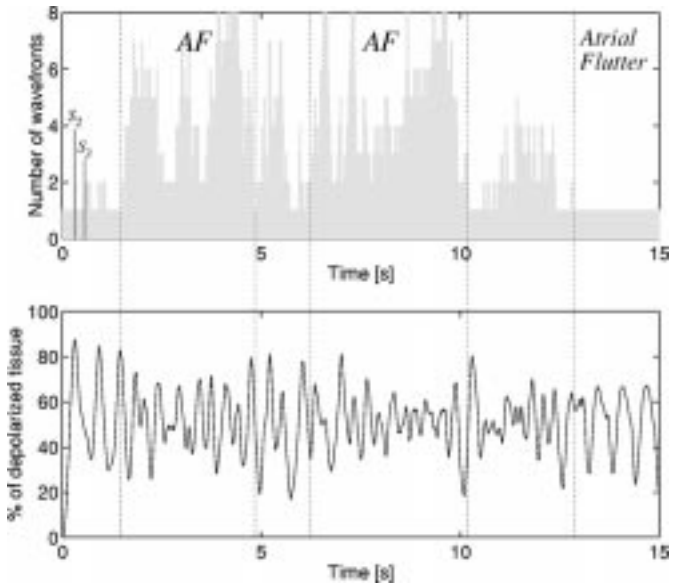

Fig. 7. Development of the number of wavelets and the percentage of excited tissue during the initiation of AF and its spontaneous transition to atrial flutter. The initiation protocol is the one described in Fig. 6. The percentage of excited tissue is defined as the amount of cardiac cells with a V_m greater than -60 mV.

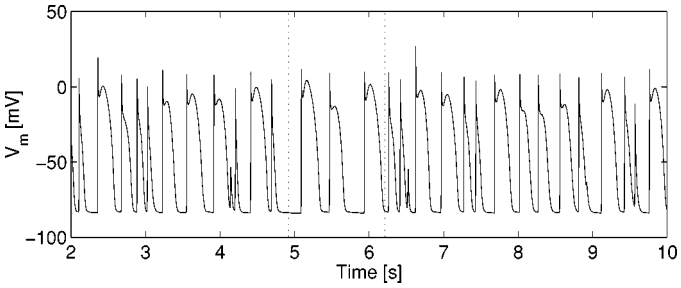

Fig. 8. Example of evolution of the transmembrane potential V_m during AF for a point located between IVC and TV. This graphic corresponds to the data presented in Figs. 6 and 7. The average rate during AF is 250 bpm.

tion to flutter. The periodicity of flutter is also visible at the end of the simulation. The evolution of the transmembrane potential V_m for a given cell is presented in Fig. 8. One can notice the higher rate obtained during AF compared to the flutter like activity between $t = 5$ and 6 s. The typical irregular pattern of fibrillation can also be observed.

One important observation is that, in our model, atrial arrhythmias are a combination of functional and anatomical reentries. The influence of the anatomy of the heart on the mechanisms of arrhythmia is clearly visible in our experiments with two opposite effects. First, orifices simulating veins and valves tend to break wavefronts or to create preferential regions for wavefront collisions (in the isthmus between IVC and TV or in the pulmonary veins). On the other hand, orifices also act as anchors for the reentrant wave and have a stabilization effect, as described in [31]. In the simulation presented in Figs. 6–8, the stimulus S_3 creates a rotor that rotates around SVC during the initiation phase of AF by two ectopic beats. After several rotations, the wave detaches itself and hits a slow recovery wavefront created by S_2, which initiates AF. Fibrillation is then sustained for a few seconds and the transition from fibrillation to a periodic and more stable reentrant wave is facilitated by the

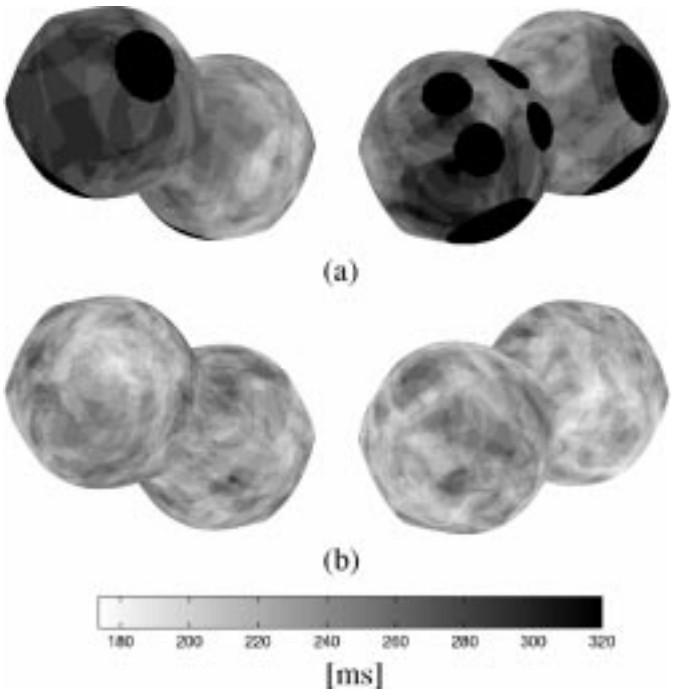

Fig. 9. Spatial distribution of activation intervals(threshold -60 mV) during AF: (a) with anatomical obstacles, computed over 8 s, (b) without anatomical obstacles, computed over 7 s, starting 1 s after anatomical obstacles are removed.

anchoring phenomenon. It seems that the vena cava play an important role in the anchoring process. Our simulations tend also to confirm the multiple wavelets hypothesis, which states that only a critical number of wavelets can maintain fibrillation [27].

We also measured the spatial distribution of activation intervals on the atrial surface during AF. Fig. 9 compares the interval distribution with and without anatomical obstacles. Fig. 9(a) illustrate how, even in a homogeneous tissue, anatomical obstacles can create a nonuniform spatial distribution of rate, with a higher rate (shorter activation interval) in the left atrium than in the right. It is interesting to observe what happens when the anatomical obstacles are removed from the tissue while AF is running, as illustrated in Fig. 9(b). We can observe a much more uniform spatial distribution of AF activation intervals (the differences between the right and left atrium disappear) and the overall rate is higher. Therefore, obstacles are important in determining the size and location of reentrant pathways, which will in turn determine the rate.

IV. Conclusion

Every model is a simplification of reality and the development described here is no exception. One limitation of the present model is the use of a simplified geometry with only one layer of cells for the atrium. This simplification, as a first approach to an atrial model, seems reasonable due to the limited thickness of the atria. This would not be the case in a ventricular model. Furthermore, only the most important anatomical obstacles (veins and valves) have been modeled here, otherwise uniform properties for the whole atrial tissue (APD and propagation speed) have been applied. The effect of this simplification is that the activation maps will not precisely match what can be found in humans. However, it is still possible

to reproduce realistic atrial arrhythmias in terms of size of reentrant circuit, global behavior of activation maps, rate, and number of wavelets. In this paper, we illustrated how atrial anatomical obstacles affect the distribution of AF intervals. Our objective was to study this effect separately from other anatomical features. The next step would be to incorporate the anisotropic structures which affect the activation patterns the most, such as crista terminalis or Bachmaan's bundle. It has been also shown that pectinate muscles play a role in activation patterns during AF [32]. Finally, we are using a ventricular action potential to simulate atrial cells. In order to compensate the fact that ventricular potentials are longer than atrial ones, in all simulations we tested APDs in a range of 113 ms to 289 ms, which covers the range of atrial APDs in normal atrium and AF [33]. Therefore, the use ventricular model probably does not significantly impact propagation properties, but makes this model inappropriate for the study of pharmacological interventions.

There have been published recently several model of human atria taking into account anatomical features [5], [6], [34]. The available computer power is comparable, but these models differ by the tradeoffs made, which are dependent on their objectives. Some of them use a reduced number of nodes in anatomical models, which is possible only with simplified cellular models due to the spatial discretization limitation, but which allows a long simulation of several seconds [5], [34]. If realistic membrane kinetics are used, the size of tissue that can be simulated or the total simulation time have to be reduced. Harrild *et al.* presented a 3-D computer model of atria using an atrial cellular model and including most of the anatomical features [6]. This model is able to precisely reproduce atrial activation maps during 1 s of normal activation. The inclusion of these refinements is however at the expense of a coarser discretization grid, an increased computational load and therefore a reduction of the total time that can be simulated. Finally, it is still not clear today what are the improvements that will affect significantly the simulations. In this case, the advantage of computer simulations over clinical experiments resides in the fact that it is possible to study separately, in controlled and reproducible conditions, the effect of these factors.

Our model has the advantage of low computational load, associated with 2-D patches, combined with a better topology usually associated with 3-D models, and a realistic size and propagation velocity. It showed how the main auricular obstacles determine critical regions for the initiation and perpetuation of atrial arrhythmias, the reentry pathways and the spatial distribution of fibrillatory rate. One factor to highlight is that, while it is possible to study normal propagation by simulating one event during 1 s, this is not the case when studying AF with a computer model. Indeed, in order to compare simulation data with clinical results from human AF, it is necessary to be able to run simulations of several seconds in different experimental conditions. In our case, we put the emphasis on running multiple (10–20) simulations of several seconds (from 5 to 40) rather than running one single simulation. Therefore, we did not use a parallel algorithm but ran simulations on up to 20 PCs in parallel for the testing of the different configurations (location and timing of ectopic beats) leading to different patterns of atrial arrhythmias (flutter, sustained or nonsustained AF). Simulations of up to 40 s have been performed requiring 5.5 days of computation time with the model of 65 000 nodes, while the results published for realistic models with a high number of cardiac cells are usually limited to 1 s due to their complexity [2]. Our goal is to use this atrial model as a tool to obtain a better understanding of the mechanisms of arrhythmias and to test therapeutic strategies like pacing, defibrillation, ablation, or drugs.

REFERENCES

[1] P. Wolf, E. Benjamin, A. Belanger, W. Kannel, D. Levy, and R. D'Agostino, "Secular trends in the prevalence of atrial fibrillation: The Framingham study," *Amer. Heart J.*, vol. 131, pp. 790–796, 1996.

[2] C. S. Henriquez and A. A. Papazoglou, "Using computer models to understand the roles of tissue structure and membrane dynamics in arrhytmogenesis," *Proc. IEEE*, vol. 84, pp. 334–354, Mar. 1996.

[3] W. Quand, S. J. Evans, and M. Hastings, "Efficient integration of realistic two-dimensional cardiac tissue model by domain decomposition," *IEEE Trans. Biomed. Eng.*, vol. 45, pp. 372–385, Mar. 1998.

[4] D. Noble and R. L. Winslow, "Reconstruction of the heart: Network models of SA node-atrial interaction," in *Computational Biology of the Heart*, A. V. Panfilov and A. V. Holden, Eds. New York: Wiley, 1997, pp. 49–64.

[5] R. A. Gray and J. Jalife, "Ventricular fibrillation and atrial fibrillation are two different beasts," *Chaos*, vol. 8, no. 1, pp. 65–78, 1998.

[6] D. M. Harrild and C. S. Henriquez, "A computer model of normal conduction in the human atria," *Circ. Res.*, vol. 87, pp. E25–E36, 2000.

[7] A. V. Panfilov, "Spiral breakup as a model of ventricular fibrillation," *Chaos*, vol. 8, no. 1, pp. 57–64, 1998.

[8] G. W. Beeler and H. Reuter, "Reconstruction of the action potential of ventricular myocardial fibers," *J. Physiol.*, vol. 268, pp. 177–210, 1977.

[9] C. Luo and Y. Rudy, "A model of the ventricular cardiac action potential," *Circ. Res.*, vol. 68, no. 6, pp. 1501–1526, 1991.

[10] M. A. Allessie, P. L. Rensma, J. Brugada, J. L. R. M. Smeets, O. Penn, and C. J. H. Kirchhof, "Pathophysiology of atrial fibrillation," in *Cardiac electrophysiology: From Cell to Bedside*, D. P. Zipes and J. Jalife, Eds. Philadelphia, PA: Saunders, 1990, pp. 548–559.

[11] J. L. Cox, R. B. Schuessler, and J. P. Boineau, "The surgical treatment of atrial fibrillation. II. Summary of the current concepts of the mechanisms of atrial flutter and atrial fibrillation," *J. Thorac. Cardiovasc. Surg.*, vol. 101, pp. 402–405, 1991.

[12] R. A. Gray, K. Takkellapati, and J. Jalife, "Dynamics of anatomical correlates of atrial flutter and fibrillation," in *Cardiac Electrophysiology: From Cell to Bedside*, D. P. Zipes and J. Jalife, Eds. Philadelphia, PA: Saunders, 1995, pp. 356–363.

[13] B. E. H. Saxberg and R. J. Cohen, "Cellular automata models of cardiac conduction," in *Theory of the Heart—Biomechanics, Biophysics and Nonlinear Dynamics of Cardiac Function*, L. Glass, P. Hunter, and A. McCulloch, Eds. New York: Springer-Verlag, 1991, pp. 437–476.

[14] R. A. FitzHugh, "Impulses and physiological states in theoretical models of nerve membrane," *J. Biophys.*, vol. 1, pp. 445–466, 1961.

[15] S. S. Demir, J. W. Clark, C. R. Murphy, and W. R. Giles, "A mathematical model of a rabbit sinoatrial node cell," *Amer. J. Physiol.*, vol. 266, pp. C832–C852, 1994.

[16] A. Nygren, C. Fiset, J. W. Clark, D. S. Lindblad, R. B. Clark, and W. R. Giles, "Mathematical model of an adult atrial cell: The role of K+ currents in repolarization," *Circ. Res.*, vol. 82, pp. 63–81, 1998.

[17] C. Luo and Y. Rudy, "A dynamic model of the cardiac ventricular action potential. I: Simulation of ionic currents and concentration changes," *Circ. Res.*, vol. 74, pp. 1071–1096, 1994.

[18] K. Skouibine, N. Trayanova, and P. Moore, "A numerically efficient model for simulation of defibrillation in an active bidomain sheet of myocardium," *Math. Biosci.*, vol. 166, pp. 85–100, 2000.

[19] N. Virag, J.-M. Vesin, and L. Kappenberger, "A computer model of cardiac electrical activity for the simulation of arrhythmias," *PACE*, pt. II, vol. 21, no. 11, pp. 2366–2371, 1998.

[20] E. Braunwald, "Valvular heart disease," in *Heart Disease, a Textbook of Cardiovascular Medicine*, E. Braunwald, Ed. Philadelphia, PA: Saunders, 1992, pp. 1007–1077.

[21] S. Y. Ho, D. Sanchez-Quintana, J. A. Cabrera, and R. H. Anderson, "Anatomy of the left atrium: Implications for radiofrequency ablation of atrial fibrillation," *J. Cardiovasc. Electrophysiol.*, vol. 10, pp. 1525–1533, 1999.

[22] M. Courtemanche, "Complex spiral wave dynamics in a spatially distributed ionic model of cardiac electrical activity," *Chaos*, vol. 6, no. 4, pp. 579–600, 1996.
[23] P. J. Hunter, B. H. Smaill, P. M. F. Nielsen, and I. J. Le Grice, "A mathematical model of cardiac anatomy," in *Computational Biology of the Heart*, A. V. Panfilov and A. V. Holden, Eds. New York: Wiley, 1997, pp. 171–215.
[24] C. F. Gerald and P. O. Wheatley, *Applied Numerical Analysis*. Reading, MA: Addison-Wesley, 1989.
[25] J. P. Keener and K. Bogar, "A numerical method for the solution of bidomain equations in cardiac tissue," *Chaos*, vol. 8, no. 1, pp. 234–241, 1998.
[26] J. Wu and D. P. Zipes, "Effects of spatial segmentation in the continuous model of excitation propagation in cardiac muscle," *J. Cardiovasc. Electrophysiol.*, vol. 10, no. 7, pp. 965–972, 1999.
[27] M. A. Allessie and M. J. Janse, "Mechanisms of atrial arrhythmias," in *Electropharmacological Control of Atrial Arrhythmias*, B. Singh and H. J. J. Wellens, Eds. Mt. Kisco, NY: Futura, 1994, pp. 115–133.
[28] J. L. Cox, T. E. Canavan, R. B. Schuessler, M. E. Cain, B. D. Lindsay, C. Stone, P. K. Smith, P. K. Smith, P. B. Corr, and J. P. Boineau, "The surgical treatment of atrial fibrillation. II. Intraoperative electrophysiologic mapping and description of the electrophysiologic basis of atrial flutter and atrial fibrillation," *J. Thorac. Cardiovasc. Surg.*, vol. 101, pp. 406–426, 1991.
[29] M. Haissaguerre, P. Jais, D. C. Shah, A. Takahashi, M. Hocini, G. Quiniou, S. Garrigueadn, A. Le Mouroux, P. Le Métayer, and J. Clémenty, "Spontaneous initiation of atrial fibrillation by ectopic beats originating in the pulmonary veins," *New Eng. J. Med*, vol. 339, no. 10, pp. 659–666, 1998.
[30] R. J. Schilling, A. H. Kadish, and N. S. Peters, "Endocardiac mapping of atrial fibrillation in the human right atrium using a noncontact catheter," *Eur. Heart J.*, vol. 21, pp. 550–564, 2000.
[31] F. Xie, Z. Qu, and A. Garfinkel, "Dynamics of reentry around a circular obstacle in cardiac tissue," *Physical Rev. E*, vol. 58, no. 5, pp. 6355–6358, 1998.
[32] E. Foster, R. A. Gray, and J. Jalife, "Role of pectinate muscle structure in atrial fibrillation: A computer study," *PACE*, pt. II, vol. 20, pp. 1134–1134, 1997.
[33] M. Courtemanche, R. J. Ramirez, and S. Nattel, "Ionic target for drug therapy and atrial fibrillation-induced electrical remodeling: Insights from a mathematical model," *Cardiovasc. Res.*, vol. 42, pp. 477–489, 1999.
[34] W. S. Ellis, A. SippensGroenewegen, and M. Lesh, "The effect of linear lesions of atrial defibrillation threshold and spontaneous termination. A computer modeling study," *PACE*, pt. II, vol. 20, pp. 1145–1145, 1997.

Olivier Blanc received the B.S. degree in mechanical engineering from the Swiss Federal Institute of Technology (EPFL), Lausanne, Switzerland). He then received the M.S. degree in biomedical engineering from EPFL and the University of Lausanne, working on nonlinear analysis of cardiovascular signals. He is now working toward the Ph.D. degree at the Signal Processing Laboratory (LTS) of EPFL, studying computer modeling of the electrical propagation in the myocardium.

Nathalie Virag received the M.S. degree in electrical engineering and the Ph.D. degree from the Swiss Federal Institute of Technology (EPFL), Lausanne, Switzerland, in 1993 and 1996, respectively. Her Ph.D. degree thesis was in the field of speech enhancement and recognition.

From 1996 to 1998, she worked as a Research Assistant at the Signal Processing Laboratory, EPFL, in the field of biomedical signal processing and computer modeling. She is currently with Medtronic in Switzerland as a Research Scientist.

Jean-Marc Vesin graduated from the Ecole Nationale Supérieure d'Ingénieurs Electriciens de Grenoble (ENSIEG), Grenoble, France, in 1980. He received the M.S. degree from Laval University, Québec City, Québec, Canada, in 1984, where he spent four years on research projects. After two years in industry, he joined the Signal Processing Laboratory (LTS) of the Swiss Federal Institute of Technology , Lausanne, Switzerland, where he received the Ph.D. degree in 1992.

Since then, he has been in charge of the activities in one-dimensional signal processing at LTS. His main interests are biomedical signal processing, nonlinear signal modeling and analysis, and the applications of genetic algorithms in signal processing.

Lukas Kappenberger received the M.D. degree in 1971 from the University of Basel, Basel, Switzerland. He received the diploma in internal medicine in 1975 and in cardiology in 1980.

From 1979 to1985, he worked in internal medicine and cardiology at the University of Zurich, Switzerland. Since 1985, he is the Head of the Division of Cardiology of the University Hospital of Canton de Vaud (CHUV), Lausanne, Switzerland.